JOURNAL OF OPTOELECTRONICS AND ADVANCED MATERIALS, Vol. 11, No. 2, February 2009, p. 169 - 174

Fabrication and properties of novel Langmuir-Blodgett films with multifunctional molecular precursors of lanthanide complexes with long chain para-L-oxybenzoate (L = 1-palmitoyl, 1-stearoyl)

BING XU[a], BING YAN[a, b*]
[a]*Department of Chemistry, Tongji University, Shanghai 200092, P. R. China*
[b]*State Key Lab of Coordination Chemistry, Nanjing University, Nanjing 210093, P.R. China*

Several ultra thin luminescent Langmuir–Blodgett (LB) films have been prepared by using the subphase containing the rare earth ions (Eu^{3+}, Dy^{3+}). The effect of the rare earth ions on the monolayer of p-palmitoyloxybenzoate (16-OBA) and p-stearoyloxybenzoate (18-OBA) was investigated. IR spectra showed the rare earth ions were bound to the carboxylic acid head groups and the coordination took place between the polar head group and the rare earth ions. The layer structure of the LB films was demonstrated by low-angle X-ray diffraction. The AFM study revealed that the LB films were uniform and crack free, and the films mainly consisted of closely packed grains with an average size of 278 nm. The LB films can give off strong fluorescence, and the signal can be detected from a single layer. The characteristic luminescence behaviors of LB films have been discussed compared with those of the complexes.

(Received July 4, 2008; accepted February 23, 2009)

Keywords: Chemical modification, Photoluminescence, Molecular fabrication, Thin films

1. Introduction

More and more attention has been paid to the studies on rare earth organic complexes for their optical, electrical and magnetic properties. Functional organized ultrathin films of these complexes which have potential applications in molecular optics and photoelectronics techniques have been fabricated by using Langmuir–Blodgett LB technique [1–3]. LB film technique has provided an extensive example for rare earth complexes molecular arrangement. In the last decade, many luminescent lanthanide complexes have been deposited as ordered ultrathin film by Langmuir–Blodgett method and their luminescence properties have been investigated [4–8]. LB films containing metal ions have uncommon electronic and magnetic properties. For the purposes, many metallic LB films made of fatty acid containing divalent metals (such as Cd^{2+}, Mn^{2+}, and Ba^{2+}) were investigated because many metallic ions are easily adsorbed along a fatty acid monolayer [9,10]. Long luminescent lifetimes and the narrow emission bands have allowed the use of rare earth cations in label technology for clinical diagnostic use, display phosphor screens, laser, electroluminescent optical devices and probes [11–14]. The assembly of rare earth materials into two-dimensional ordered LB films may have the potential applications such as molecular magnetic and optical storage or chemically functionalized superconducting switches for molecular films. Fanucci and Talham prepared several metal phosphonate LB films based upon solid-state lanthanide (III) phosphaonates by Y-type deposition procedure [15]. Osvaldo et al. [9] deposited some compounds as LB films which reacted with europium ion and ligands, concluding that the films fabricated gave off strong fluorescence emission. Huang et al. [16-17] combined rare earth anions with some organic molecules with nonlinear optical properties and found that the rare earth complex anions not only optimize the formation of the multilayers but also enhance the nonlinear optical efficiency of the organic molecules. The film formation function and luminescent sensitization function are the crux of LB film construction; however the two functions are separated at most time. In this context, p-palmitoyloxybenzoate (16-OBA), p-stearoyloxybenzoate (18-OBA) undertook the two double function of film-forming and luminescent sensitization.. The IR, UV and luminescence spectra data indicated that the lanthanide metal cations were bound with the head groups of 16-OBA and 18-OBA. The experimental results indicate the system can be used for the preparation of ultrathin films with high luminescent properties. The new type of LB films may be used for the application as sensors and photoelectrochemical devices.

2. Experimental details

2.1. Materials

p-palmitoyloxybenzoate (16-OBA) and p-stearoyloxybenzoate (18-OBA) were synthesized as the literature [18], and confirmed by NMR and MS spectra. $LnNO_3 \cdot 6H_2O$ (Ln = Eu or Dy) were obtained by dissolving Eu_2O_3 or Dy_2O_3 in concentrated HNO_3 solution that was then evaporated to dryness.

2.2. Measurements

UV-visible spectra were recorded on an Agilent 8453 spectrophotometer. Infrared spectroscopy with KBr pellets was performed on a Nicolet Nexus 912 AO446 model spectrophotometer in the 4000 ~ 400 cm^{-1}. The fluorescence (excitation and emission) spectra were determined with Perkin-Elmer LS-55 spectrophotometer: excitation slit width = 10 nm, emission slit width = 5nm. X-ray diffraction data were obtained on a Rigaku D/max-γB X-ray diffractometer.AFM measurements were carried out in tapping mode with a scanning frequency of 1–2 Hz. Roughness was calculated as root-mean-square (rms) values.

2.3. Preparation of LB films

A computer-controlled (KSV5000) Langmuir trough was used for the measurement of π-A isotherm and the fabrication of LB films. The solutions of 16-OBA and 18-OBA in chloroform (1×10^{-4} mol/L) were spread onto a variety of aqueous subphase containing Ln^{3+} (Eu^{3+} or Dy^{3+}). The subphase was appropriately buffered with $NaHCO_3$ (10^{-4} mol/L). After evaporation of the solvent, the prepared monolayer was transferred onto a substrate by the vertical depositing method in Z-type model at a speed of 10 mm/min. The films were transferred onto substrates at a surface pressure of 35 mN/m on CaF_2 (for IR transmission measurements) or quartz plate (for UV, luminescence spectroscopy measurements) at the dipping speeds of 5 mm /min. The transfer ratios of the films were around unity. The substrate for the emission measurements was a nonfluorescent quartz plate (10× 30 mm). It was cleaned with sulfuric acid, dipped into 10 % hydrogen peroxide solution and then rinsed with water.

3. Results and discussion

3.1. π-A isotherms of monolayers

The surface pressure-area isotherms (π-A isotherms) for the two long chain compound on pure water and on Ln^{3+} (Ln = Eu, Dy) subphase are shown in Fig. 1. In Fig. 1(a), we can see that the 16-OBA isotherm on pure water corresponds to a liquid expanded state of the lipid at the gas–water interface, and the collapse pressure is about 42 mN/m. This may be due to the strong repulsion between the head groups of 16-OBA. The addition of Ln^{3+} ions to the subphase has a great effect on the monolayer behavior of 16-OBA. When the Ln^{3+} ions are dissolved in the subphase, the π-A isotherms clearly shifts toward a smaller area per molecule compared with that on pure water. At the same time, the isotherm is steeper at the end of compression and the collapse pressure becomes higher (around 50 mN/m).

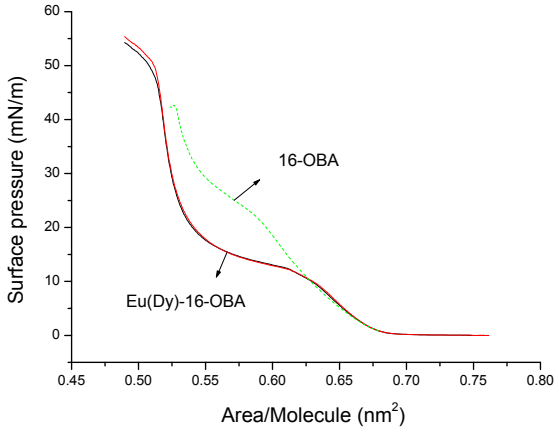

(a)

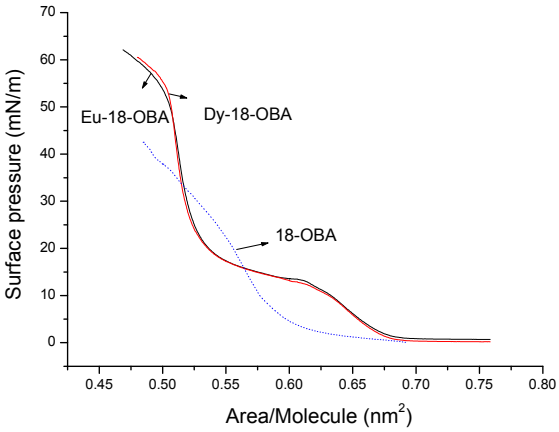

(b)

Fig. 1 π-A isotherms of 16-OBA and Ln-16-OBA (a), 18-OBA and Ln-18-OBA(b)

The smaller limiting molecular area were 0.54 and 0.54 nm^2 per molecule for Dy-16-OBA and Eu –16-OBA, which were obtained from the π-A isotherms curve by extrapolating the condensed region to zero pressure. The decrease of the limiting areas and the increase of collapse pressure of the monolayer imply the binding between the monolayer and rare earth ions in the subphase. The exactly similar molecular structures conform to the similar shapes of the π-A isotherms, excepting the small difference of the

molecular areas which isdue to the difference of the two central ions of the rare earth complexes. In Fig. 1(b), we can observe that the 18-OBA isotherm on pure water presents a liquid expanded state of the lipid at the gas–water interface. When the Ln^{3+} ions are dissolved in the subphase, the π-A isotherms also shifts toward a smaller area per molecule compared with that on pure water and have the exactly similar shape for Dy-18-OBA and Eu–18-OBA. The molecular area was 0.53 nm^2 per molecule. The decrease of the limiting areas and the increase of collapse pressure of the monolayer mean the combining between the monolayer and rare earth ions in the subphase [19]. The surface behavior observed on Ln^{3+} subphase could be due to the adsorption of Ln^{3+} along the charged head groups, which counterbalance the repulsion between the head groups. The π-A isotherms of the two long chain ligand on the Ln^{3+} (Ln = Eu, Dy) subphase are similar, which indicates that the effect of the two kinds of cations on the two ligands is similar. The similarity of surface behaviors reflects the similarity and continuity of their chemical and physical properties of the two lanthanide elements of Dy and Eu.

3.2. IR spectra

IR spectra of ligands and complexes film were measured. For the Dy-16-OBA LB film, the characteristic absorption peaks of carboxylic group COO^- appear 1550cm^{-1} for vas(COO-) and 1465 for vs(COO-), respectively) while there does not exist for free 16-OBA, suggesting that the oxygen atoms of 16-OBA carbonyl group are coordinated with Ln^{3+} in LB film. Both the 16-OBA and Dy-16-OBA LB film show the characteristic absorption bands of carbonyl group (1704.42 cm^{-1} (strong) for 16-OBA and 1734.42 cm^{-1} for Dy-16-OBA LB film except for the weaker absorption intensity for complexes than that of 16-OBA, which suggests that there still exist one carboxyl group of long chain carboxyphenol ester and these carbonyl groups coordinated with Dy^{3+} ions for the absorption band shift to low frequency. In the IR spectra of Eu-18-OBA LB film, the characteristic absorption peaks of carboxylic group COO^- appear 1540 cm^{-1} for vas(COO-) and 1411 cm^{-1} for vs(COO-), respectively while it is not observed for free 18-OBA ligand, indicating that the oxygen atoms of 18-OBA carbonyl group are coordinated with Eu^{3+}. Both the free ligand and its complexes show the characteristic absorption bands of carbonyl group (1705.52 cm^{-1} (s) for 18-OBA and 1670.79 cm^{-1} for Eu-18-OBA LB film except for the weaker absorption intensity for complexes than that of 18-OBA, which indicates that there still exist one carbonyl group of long chain carboxyphenol ester which also take part in coordination with Ln ions for the absorption band shift to low frequency.

3.3. UV-Visible absorption spectra and low-angle X-ray diffraction

The UV-visible absorption spectra are shown in Fig. 2. In Fig.2(a), the Eu-16-OBA LB films and 16-OBA LB film have peak at same position (199 nm), while 16-OBA solution has the maximal peak located at 248 nm (π → π* transition) , It could be concluded that the peak around 199 nm in LB films come from the 16-OBA, specifically, it can be ascribed to the π → π* transition of phenyl ring with long-chain substituted group, which shift greatly to lower wavelength in LB film compared with its solution.. In Fig. 2(b), the situation was same as Fig.2(a). The 18-OBA solution has maximal absorption peak at 243 nm, which caused by π → π* transition of phenyl ring. When Dy-18-OBA was transferred onto quartz plate, the maximal absorption appeared at 197 nm, at the same time the 18-OBA LB films also has strong absorption around 198 nm. Hence, the absorption peak turned up in Dy-18-OBA LB film come from the π → π* transition of phenyl ring of the 18-OBA. These phenomena can be endorsed indeed to the film interactions and to the ordered arrangement of the molecules in the film. The molecules in the solution are present as free single molecules, and the interactive forces among them can be neglected, but the molecules in the LB film are in an aggregate state with strong interactions.

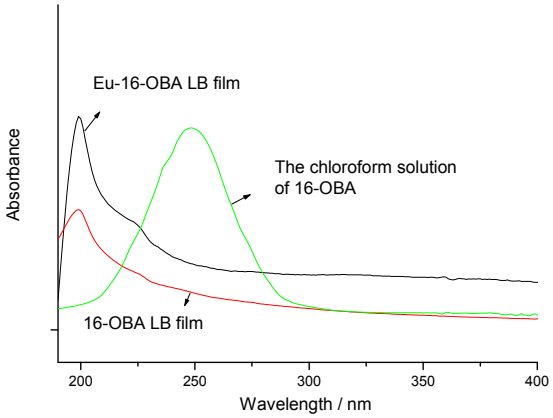

(a)

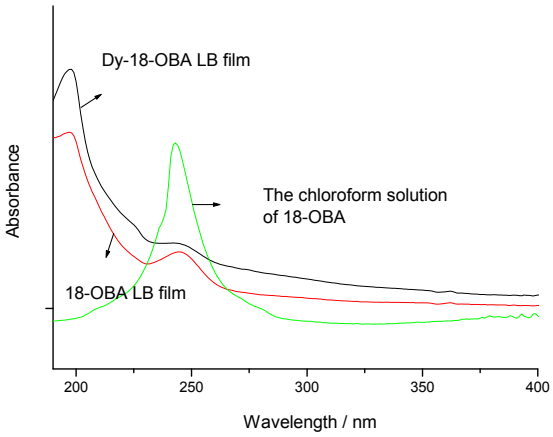

(b)

Fig. 2 Ultraviolet-visible absorption spectra of 16 layer Eu- 16-OBA LB film, 16-OBA in chloroform and in LB film (a); 15layer Dy- 18-OBA LB film, 18-OBA in chloroform and in LB film (b).

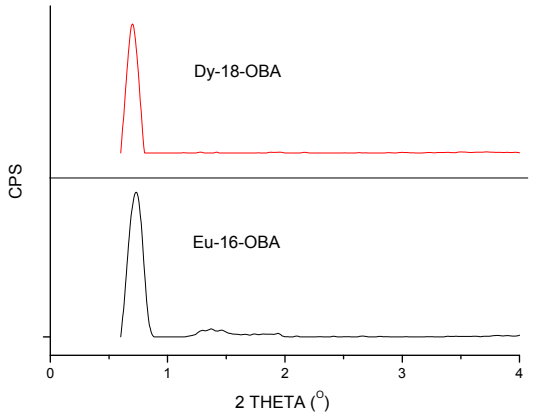

Fig. 3 Low-angle X-ray diffraction of 16 layers LB film of Eu- 16-OBA and 15layer LB film of Dy- 18-OBA.

The low-angle X-ray diffractograms of Ln-16-OBA and Ln-18-OBA LB films on quartz plates are shown in Fig. 4. The regular X-ray diffraction pattern points out that these LB films have ordered structure. For 14 layers of Eu-16-OBA LB film, It exhibits evident diffraction peaks at 0.72 ˚ and 1.368 ˚, which is assigned to be (001) and (002) Bragg diffraction respectively. The average layer spacing of 8.75 Å is determined according to the Bragg equation [20]. For 13 layers of Dy-18-OBA LB film, two diffraction peak appear at 0.714 ° (001), from which the average layer spacing was calculated to be 10.48 Å. It is clear that the average layer spacing increases with the increase of ligand length.

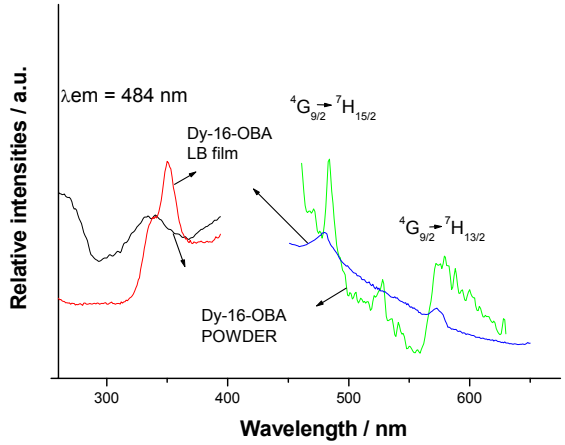

Fig. 4 Excitation and emission spectra of Dy-16-OBA LB film and corresponding powder.

3.4. Luminescence properties

The excitation bands and emission bands for Dy-12-OBA LB film and corresponding powder were shown in Fig. 4. Under the blue emission of 484 nm, the Dy-16-OBA LB film present the maximum excitation peaks around 349 nm. The excitation spectrum of Dy-16-OBA complex powder shows a different broad band with the peaks at 333 and 342 nm, shifting to lower energy region compared with that of the complex LB films. When Dy-16-OBA LB film was excited under 350 nm, two characteristic fluorescence emission peaks of Dy^{3+} around 480 and 573 nm were obtained, corresponding to $^4G_{9/2}\rightarrow{}^7H_{15/2}$ (B) and $^4G_{9/2}\rightarrow{}^7H_{13/2}$ (Y) transitions respectively, [21], The intensity ratio of Y and B values of the LB film is 0.474. For Dy-16-OBA complexes powder, under the excitation of 330 nm, the luminescence spectra show two apparent emission peaks: one is at 483 nm ($^4G_{9/2}\rightarrow{}^7H_{15/2}$), and the other is at 574 nm ($^4G_{9/2}\rightarrow{}^7H_{13/2}$). The intensity ratio of Y and B values of the solid is 0.523. In Fig. 5, the Dy-18-OBA LB film have the maximum excitation peaks at 344 nm under the emission of 484nm, while the Dy-18-OBA powder show a broad band from 220 to 361 nm without apparent peaks. At the excitation of 350 nm, the emission spectrum of the Dy-18-OBA LB film consists of two bands, corresponding to the transitions $^4G_{9/2}\rightarrow{}^7H_{15/2}$ (479 nm) and, $^4G_{9/2}\rightarrow{}^7H_{13/2}$ (571 nm). The Y: B value of the LB film is 0.556. The emission spectra of Dy-18-OBA powder consists of two characteristic luminescence emissions of Dy^{3+} around 481, 576, which correspond to $^4G_{9/2}\rightarrow{}^7H_{15/2}$, $^4G_{9/2}\rightarrow{}^7H_{13/2}$ transitions. The Y: B value of the solid is 1.235, which is bigger than that of LB films. The shapes of the luminescence spectra and the intensity ratio between the $^4G_{9/2}\rightarrow{}^7H_{15/2}$ and $^4G_{9/2}\rightarrow{}^7H_{13/2}$ transition are different between LB films and solids. On analyzing the experimental results in the emission spectra, we think that the yellow emission of $^4G_{9/2}\rightarrow{}^7H_{13/2}$ of Dy^{3+} is hypersensitive and is influenced strongly by the outside surroundings. The interactions between molecules may be changed compared with that of powder and cause the distortion in the symmetry of the molecules. The transition probability between energy levels might be changed when the symmetry of molecular structure is different. The ordered packing of molecules in LB films also contributes to the fluorescence emission.

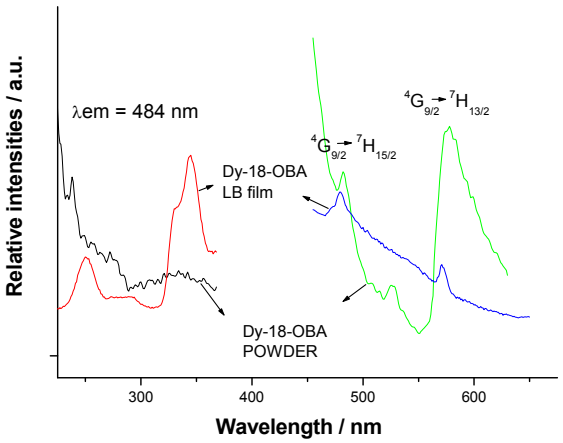

Fig. 5 Excitation and emission spectra of Dy-16-OBA LB film and corresponding powder.

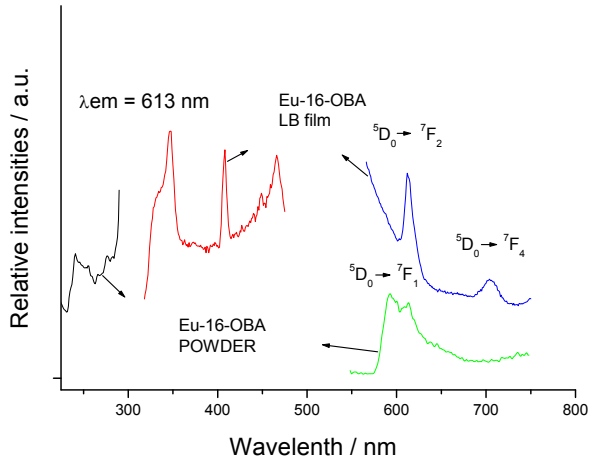

Fig. 6 Excitation and emission spectra of Eu-18-OBA LB film and corresponding powder.

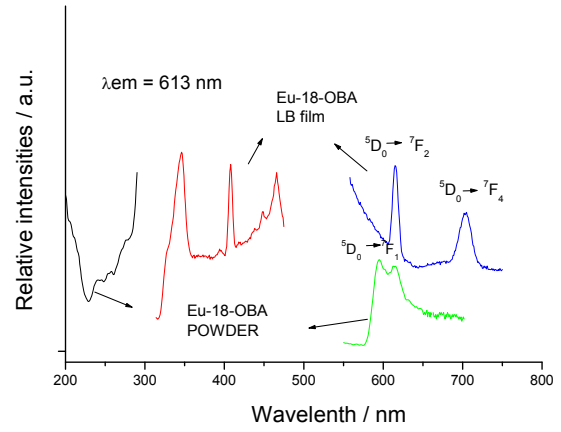

Fig. 7 Excitation and emission spectra of Eu-18-OBA LB film and corresponding powder.

The excitation and emission spectra of Eu-16-OBA and Eu-18-OBA are shown in Figs. 6 and 7. In Fig, 6, the excitation spectrum of Eu–16-OBA powder was obtained by monitoring the emission of Eu^{3+} at 613 nm and dominated by a distinguished band centered at 242 nm, which leads to $^5D_0 \rightarrow {}^7F_1$ and $^5D_0 \rightarrow {}^7F_2$ of Eu^{3+} at 593 and 613, respectively. The two emission bands have overlap in most area, suggesting that the long chain carboxyphenol ester could not sensitive Eu^{3+} ion sufficiently. The excitation spectra of Eu–16-OBA LB film is measured under an emission wavelength of 613 nm and consists of several bands (347, 408 and 467nm)in the long ultraviolet region, which would be contributed to intraconfigurational 4f→4f transitions from the ground $^7F_0$ level, The emission spectra of Eu –16-OBA LB film present great different compared with that of power. Under the excited of 408 nm, there are two apparent peak turned up at 613 and 704 nm, which corresponding to $^5D_0 \rightarrow {}^7F_2$ and $^5D_0 \rightarrow {}^7F_4$ transition of Eu^{3+} respectively, while the most important magnetic dipolar transition of $^5D_0 \rightarrow {}^7F_1$ disappeared. In Fig. 7, the excitation spectrum for Eu –18-OBA powder consists a broad band with three peaks at 238, 255 and 276 nm, the corresponding emission spectrum contains $^5D_0 \rightarrow {}^7F_j$ (J= 1, 2) transition lines of Eu^{3+}, similarly, the ligand could not transfer energy to Eu^{3+} ion sufficiently because the two emission bands of Eu^{3+} locating at 595 and 613 nm also have overlap.

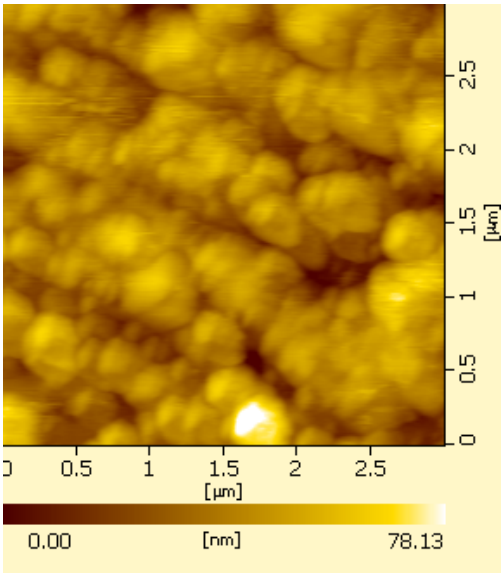

8(a)

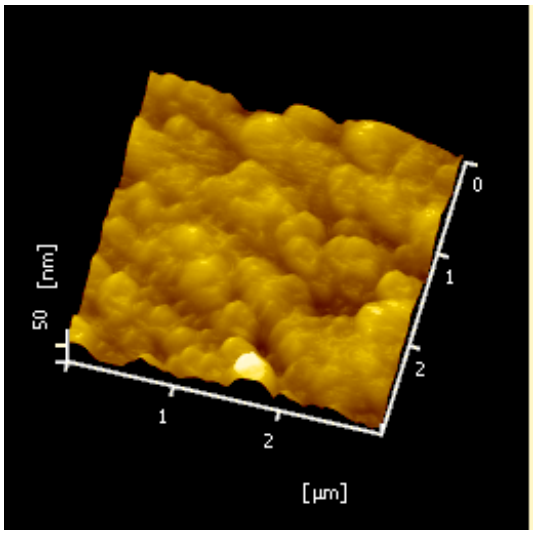

8(b)

Fig. 8 AFM images of the transparent Eu-18-OBA LB film: (a) planar image; (b) stereo v image.

The excitation spectrum of Eu –18-OBA LB film consists three bands in the long wavelength period, as a result, two peaks assigned to the $^5D_0 \rightarrow ^7F_2$ and $^5D_0 \rightarrow ^7F_4$ transitions of Eu^{3+} were obtained in the emission spectrum of the LB films, which located at 615 and 703 nm dividedly. As we know, the induced electrical dipole transition $^5D_0 \rightarrow ^7F_2$ of Eu^{3+} is hypersensitive to the surrounding of Eu^{3+} and the larger the ratio of intensity of $^5D_0 \rightarrow ^7F_2$ / $^5D_0 \rightarrow ^7F_1$ is, the more symmetrical the local sites of Eu^{3+} is. In our two LB films, the peak of $^5D_0 \rightarrow ^7F_1$ transition were entirely absent which show that the Eu^{3+} is bonded within low symmetry local sites (without inversion center) and the packing of LB films force the molecule to array in some order, which could squeeze molecules and result in lower symmetry.

3.5. Morphology of the film

The morphology of the Eu–18-OBA LB film sample was inspected using an atomic force microscope (AFM). The AFM image of the transparent film is shown in Figure 8. It is known from that planar image that the film, which is uniform and crack-free, mainly consists of closely packed fine particles with an average grain size of 278 nm (Figure 8a). The film surface is very smooth with a root mean square (RMS) roughness of 12.43 nm (stereo image in Figure 8b).

4. Conclusions

Ultrathin films of the carboxyphenol ester-rare earth have been prepared by LB technique. The layer structure of the LB films was demonstrated by low-angle X-ray diffraction. The LB films were studied by UV, IR and luminescence spectra. LB films containing Ln^{3+} (Eu^{3+}, Dy^{3+}) can give off the strong luminescence. The luminescence properties of LB films were discussed in details compared with the corresponding complexes powder. The luminescence data show that the long chain carboxyphenol ester ligands can effectively transfer energy to rare earth ions in the LB films.

Acknowledgements

This word was supported by the National Natural Science Foundation of China (20671072).

References

[1] Y.Q. Liu, K. Shigehara, M. Hara, A. Yamada, J. Am. Chem. Soc. **113,** 440 (1991).
[2] C.L. Medeiros, O.A. Serra, M.E.D. Zaniquelli, Thin Solid Films **248**, 115 (1994).
[3] D.J. Qian, K.Z. Yang, Acta Phys. Chem. Sin. **9**, 148 (1993).
[4] L. Hui, C. H. Huang, X. S. Zhao, X. M. Xie, L. G. Xu, T. K. Li, Langmuir **10**, 3794 (1994).
[5] Y.L. Zhao, D.J. Zhou, C.H. Huang, Langmuir **14**, 417 (1998).
[6] Y.Huang, A. Yu, C.H.Huang, Adv. Mater. **11**, 627 (1999).
[7] O.A. Serra, I.L.V. Rosa, C.L. Medeiros, J. Lumin. **6061**, 112 (1994).
[8] R.J. Zhang, K.Z. Yang, Langmuir **13**, 7141 (1997).
[9] S. Bettarini, F. Bonosi, G. Gabrielli, G. Martini, M. Puggelli, Thin Solid Films **42**, 210 (1992).
[10] X. Peng, H. Chen, S. Kan, Y. Bai, T. Li, Thin Solid Films **242**, 118 (1994).
[11] G.E. Buono-core, H. Li, B. Marciniak, Coord. Chem. Rev. **99**, 55 (1990).
[12] V. Bekiari, P. Lianos, Adv. Mater. **10**, 1455 (1998).
[13] J. Kido, H. Hayase, K. Hongawa, K. Nagai, Appl. Phys. Lett. **65**, 2124 (1994).
[14] F.S. Richardon, Chem. Rev. **82**, 541 (1982).
[15] G. E.Fanucci, D. R.Talham, Langmuir **15**, 3289 (2000).
[16] C. H. Huang, K. Z. Wang, G. X. Xu, X. S. Zhao, X. M. Xie, L.G. Xu, T. K. Li, Langmuir **10**, 1910 (1994).
[17] C. H. Huang, K. Z. Wang, G. X. Xu, X. S. Zhao, X. M. Xie, Y. Xu, Y. Q. Liu, L.G. Xu, T. K. Li, J. Phys. Chem. **99,** 14397 (1995).
[18] B Xu, B Yan, Spectrochim. Acta, A. **66**, 1115 (2007).
[19] H. G. Liu, W. Z. Lan, K.Z.Yang, Z. G. Yun, H.W. Zhang, Thin Solid Films **323,** 235 (1998).
[20] A. Yu, I. V. Koksharova, A. P. Bykovb, S. N. Malakhoc, G. B. Polyakovd, J. Khomutova, Bohre. Mater. Sci. Eng. C, **22**, 201 (2002).
[21] N. Kuramoto, S. Enomoto, Y. Ozaki, Langmuir **11**, 2195 (1995).

*Corresponding author: byan@tongji.edu.cn